# Efficient subset simulation for evaluating the modes of improbable slope failure

van den Eijnden, A.P.; Hicks, M.A.

**DOI**
10.1016/j.compgeo.2017.03.010

**Publication date**
2017

**Document Version**
Submitted manuscript

**Published in**
Computers and Geotechnics

**Citation (APA)**
van den Eijnden, A. P., & Hicks, M. A. (2017). Efficient subset simulation for evaluating the modes of improbable slope failure. *Computers and Geotechnics*, *88*, 267-280. https://doi.org/10.1016/j.compgeo.2017.03.010

# Efficient subset simulation for evaluating the modes of improbable slope failure

A.P. van den Eijnden[a], M.A. Hicks[a]

[a]*Section of Geo-Engineering, Faculty of Civil Engineering and Geosciences, Delft University of Technology, 2600 GA Delft, The Netherlands*

**Abstract**

For analysing low probability slope failures, a modified version of subset simulation, based on performance-based subset selection rather than the usual probability-based subset selection, is combined with the random finite element method. The application to an idealized slope is used to study the efficiency and consistency of the proposed method compared to classical Monte Carlo simulations and the shear strength reduction (SSR) method. Results demonstrate that failure events taking place without strength reduction have different modes of failure than stable slopes brought to failure by SSR. The correlation between sliding volume and factor of safety is also demonstrated.

*Keywords:* mode of failure, random finite element method, slope reliability, subset simulation

## 1. Introduction

Taking account of uncertainty in slope stability analysis typically leads to a probability distribution of failure as a function of the factor of safety. Uncertainty can reside in different aspects of the analysis (e.g., problem geometry, material parameters, and so on). A stochastic description of the parameters allows the uncertainties to be accounted for in the numerical model of the slope. The stochastic characterization of the parameters through probability density functions introduces a multidimensional sampling space filled with all possible combinations of parameter values sampled from their marginal distributions. This sampling space is ideally spanned by a set of orthogonal vectors representing the independent parameters of the stochastic characterization. The probability of failure in slope stability analysis then comes down to integrating the probability density function over the failure domain of the sampling space.

As the deterministic function of the slope stability analysis is generally non-analytical, an exact integration procedure does not exist and a numerical approximation is required. Several numerical integration techniques have been proposed for this purpose, including deterministic methods such as the point estimate method (Rosenblueth, 1975; Christian and Baecher, 1999), and the first and second order reliability methods (FORM and SORM respectively) (Baecher and Christian, 2005). These methods usually rely on a certain level of 'regularity' of the deterministic function and require the number of (independent) variables to be low.

When spatial variability is involved as part of the uncertainty, the number of independent variables for fully characterizing the distribution of material properties over the (discretized) domain of the model increases dramatically. The spatial variability is accounted for by means of random fields of material properties or state. In general, the number of variables related to spatial variability is the number of spatially varying quantities multiplied by the number of cells used for the discretization of the random field. With the increasing number of independent variables involved in the model, many numerical integration schemes can no longer integrate over the full sampling space due to the excessive computational load it would require. Moreover, the non-linearity of the deterministic function generally prevents the application of deterministic numerical methods and statistical integration methods, including the different versions of Monte Carlo simulation (MCS), form the remaining option for approximating the integral over the sampling space.

The application of MCS to slope stability problems is rather straightforward and often cast into the framework of the random finite element method (RFEM) (Griffiths and Fenton, 2004). This method has been successfully applied in slope stability analysis accounting for spatial variability in 2D (Hicks and Samy, 2002) and 3D (Hicks and Spencer, 2010). In all these applications, MCS is used to sample from the entire sampling space following the marginal distribution in each dimension. This method of crude MCS becomes inefficient when the focus is on a small probability

## Nomenclature

| | |
|---|---|
| $CoV$ | coefficient of variation |
| $E$ | Young's modulus |
| $F$ | failure event |
| $FOS_i$ | factor of safety for realization $i$ |
| $K^{(i)}$ | max. number of Markov steps per chain in subset $(i)$ |
| $K_{cl}$ | number of clusters in KMCM |
| $N$ | number of realizations |
| $N_c$ | conditional number of realizations, number of Markov chains |
| $N_t$ | total number of realizations |
| $R$ | residual term |
| $V$ | domain volume |
| $X(\vec{x})$ | random field |
| $Z$ | normalized distance from mean value (standard score) |
| $Z(\vec{x})$ | standard normal random field |
| $\Omega$ | domain |
| $\bar{\gamma}$ | variance reduction factor |
| $\gamma$ | Markov chain correlation factor |
| $\lambda^i$ | $i^{th}$ eigenvalue |
| $\mu$ | mean |
| $\mu_{LN}$ | mean of logarithm |
| $\nu$ | Poisson's ratio |
| $\sigma$ | standard deviation |
| $\sigma_{LN}$ | standard deviation of logarithm |
| $\tau$ | distance normalized against $\vec{\theta}$ |
| $\vec{\theta}$ | scales of fluctuation |
| $\vec{c}^{\,k}$ | average nodal displacement vector of cluster $k$ |
| $\vec{u}$ | (nodal) displacement vector |
| $\vec{x}$ | spatial coordinate vector |
| $c_u$ | cohesion (undrained shear strength) |
| $f_s^{end}$ | final/target strength reduction factor |
| $f_s$ | strength reduction factor |
| $m$ | total number of subdivision levels |
| $n$ | number of cells, sample space dimension |
| $p_0$ | (target) conditional probability |
| $p_f$ | probability of failure |
| $z(\vec{x})$ | random field value at position $\vec{x}$ |
| $\Psi(.)$ | (lognormal) distribution transformation function |
| $\rho(.)$ | correlation function |
| $\rho(\Omega_A, \Omega_B)$ | correlation between domains $A$ and $B$ |
| $q(.)$ | prior distribution (standard normal) |
| $\boldsymbol{I}(f_s)$ | binary failure indicator column vector |
| $\boldsymbol{X}$ | discretized random field column vector |
| $\boldsymbol{Z}$ | standard normal random field column vector |
| $\boldsymbol{\phi}^i$ | eigenvector $i$ |
| $\boldsymbol{\theta}$ | standard normal realization sample |
| $\boldsymbol{\xi}$ | standard normal random number column vector |
| $\boldsymbol{\xi}^{01}$ | uniform random number column vector |
| $\boldsymbol{\xi}^{Ms}$ | random Markov step column vector |
| E[.] | expectation operator |
| P(.) | probability operator |
| $\mathbf{A}$ | $n \times n$ matrix |
| $\mathbf{\Lambda}$ | diagonal matrix of eigenvalues |
| $\mathbf{\Phi}$ | matrix of eigenvectors |
| $\mathbf{C}$ | covariance matrix |
| $\mathbf{L}$ | lower triangle Cholesky factor |
| $[.]^\intercal$ | transpose |
| $[.]^p$ | proposal |
| $[.]^r$ | reduced |
| $[.]^s$ | seed |
| $[.]^{(i)}$ | subset level $i$ |
| $[.]^{MCS}$ | Monte Carlo simulation |
| $[.]^{SS}$ | subset simulation |
| $[.]^{end}$ | final/target |
| $[.]_L$ | lower bound |
| $[.]_U$ | upper bound |
| $[.]_i$ | index of dimension or realization number |
| $[.]_n$ | normalized against number of FEM calls |
| $\bar{[.]}$ | spatial average |
| $\hat{[.]}$ | estimation |
| CMD | covariance matrix decomposition |
| DSA | direct stability analysis |
| EOLE | expansion optimal linear estimation |
| FEM | finite element method |
| KMCM | $K$-means clustering method |
| LAS | local average subdivision |
| LEM | limit equilibrium method |
| MCMC | Markov chain Monte Carlo |
| MCS | Monte Carlo simulation |
| MMA | modified Metropolis-Hastings algorithm |
| PDF | probability distribution function |
| RFEM | random finite element method |
| SS | subset simulation |
| SSR | shear strength reduction |

event which occupies only a small part of the sampling space, whereas more advanced sampling strategies may lead to a higher sampling density close to the domain of interest.

Recently, Li et al. (2016b) applied subset simulation (SS) to the modelling of small probability failure events of slopes in spatially varying soil, in which the strength reduction method was used to determine the factor of safety of each realization in the simulation. This approach determines the required ranking of the conditional simulations in order to select the next conditional subset. The need for applying the strength reduction method in each realization introduces a computational load significantly larger than when analyzing the stability of a slope for a given level of strength reduction. A possible alternative that bypasses the strength reduction method in SS can significantly improve the efficiency of the total analysis.

This paper aims at slope stability analysis for factors of safety corresponding to low probability of failure. The factor of safety $FOS$ is here based on the shear strength reduction method and defined as the factor by which the shear strength of the material needs to be reduced to trigger failure. Note that $FOS$ is a realization-specific property of the

slope, whereas the strength reduction factor $f_s$ is a simulation parameter against which $FOS$ is compared.

## 2. Slope stability analysis using the random finite element method

The random finite element method (RFEM) (Griffiths and Fenton, 2004) is used to evaluate the reliability of a slope with spatially variable strength. The framework of RFEM can be subdivided into three parts:

- generating a series of realizations, according to the stochastic characterization of the problem under consideration;
- evaluating the response of the deterministic function for each realization;
- translating the resulting factors of safety $FOS$ to the reliability of the slope.

This framework was used to model slopes constructed in cohesive soils (Hicks and Samy, 2002; Griffiths and Fenton, 2004), cohesive-frictional soils Griffiths et al. (2009), and taking account of both saturated and unsaturated behaviour (Arnold and Hicks, 2011).

Cohesive soils are considered here, by employing a linear elastic perfectly plastic constitutive behaviour with a Tresca failure surface. The material parameters characterizing locally the constitutive relation are Young's modulus $E = 100$ MPa, Poisson's ratio $\nu = 0.3$ and cohesion $c_u$ [kPa]. The cohesion here represents the undrained shear strength of the soil and is the only parameter for which spatial variability is accounted for. This means that the undrained shear strength is a function of the spatial coordinates, $c_u = c_u(\vec{x})$. It is here assumed that $c_u$ follows a lognormal distribution with a mean of 32 kPa and a coefficient of variation of 0.25. Moreover, $c_u(\vec{x})$ is considered to be stationary (i.e., the mean and standard deviation are constant).

In the evaluation of slope reliability using RFEM, two approaches can be followed:

- **Shear strength reduction (SSR):** This technique is used to evaluate the factor of safety. The stability of a slope (failure or no failure) is evaluated for a series of iteratively updated strength reduction factors $f_s$ that reduce the strength of the soil to $c_u^r(\vec{x}) = c_u(\vec{x})/f_s$. The failure criterion is based on the required number of equilibrium iterations to obtain a converged solution of the boundary value problem (Smith et al., 2013). The lowest strength reduction factor $f_s$ to induce failure is considered to be the factor of safety for the realization of the slope. By applying SSR on a series of realizations of random fields $c_u(\vec{x})$ in a MCS, a cumulative distribution function of $FOS$ is found, characterizing the reliability of the slope.
- **Direct stability analysis (DSA):** The stability of the slope is tested against a single strength reduction factor (a meaningful choice would be $f_s = 1.00$) with a binary result; the slope is stable or the slope fails. Stability can be tested at a desired level of strength reduction and the outcome of the direct stability analysis of a realization $i$ is denoted by the indicator $I_i(f_s)$:

$$I_i(f_s) = \begin{cases} 1, & \text{if} FOS_i \leq f_s \quad \text{(failure)} \\ 0, & \text{if} FOS_i > f_s \quad \text{(no failure)} \end{cases} \tag{1}$$

The probability of failure $p_f$ is estimated from a series of $N$ realizations in a MCS as

$$p_f(f_s) = \frac{1}{N} \sum_{i=1}^{N} I_i(f_s) \tag{2}$$

## 3. Random field discretization in finite element analysis

The common practice in generating a stationary random field $X(\vec{x})$ is to construct standard normal random field $Z(\vec{x})$ and apply a transformation $\Psi(.)$ to obtain the desired distribution function for stochastic variable $X$. Generating a random field $X(\vec{x})$ with a lognormal distribution would be constructed as

$$X(\vec{x}) = \Psi(Z(\vec{x})) = \exp\left(\mu_{LN} + \sigma_{LN} Z(\vec{x})\right), \qquad \forall\ \vec{x} \in \Omega \tag{3}$$

in which the spatial correlation is accounted for in the standard normal random field $Z(\vec{x})$.

The transformation from standard normal fields provides flexibility in generation and manipulation of the random fields and several procedures have been proposed. A description and evaluation of some early algorithms for generating approximations of random fields can be found in Vanmarcke (1983) and Fenton (1994). Of particular note is the local average subdivision method (Fenton and Vanmarcke, 1990), because of its high efficiency and widespread use in geotechnical engineering (Hicks and Samy, 2002; Fenton and Griffiths, 2002; Griffiths and Fenton, 2004; Hicks and Spencer, 2010)).

Other, more exact methods can be found in various techniques based on covariance matrix decompositions, including Karhunen-Loève decomposition (Huang et al., 2001), EOLE (Li and Der Kiureghian, 1993) and sequential Gaussian methods (Deutsch and Journel, 1998). Several of these methods have found their way into the field of geotechnics for generating random fields describing the spatial variability of a range of soil parameters (e.g. Huang et al. (2013); Green et al. (2015); Suchomel and Mašín (2011)). Of particular interest with respect to subset simulation are the methods of covariance matrix decomposition, because of their ability to describe the correlated random field (after discretization) as a linear function of a set of uncorrelated standard normal variables. As such, these methods can be used to describe the discretization with few restrictions on mesh discretization or spatial correlation kernel using a minimum of variables to capture the exact spatial variation of strength parameters.

Discretization of the random field requires the translation of the continuous random field into a discretized form with a reduced number of values as parameter input for computations in the RFEM framework. As the random field will be used in the FE computations, the maximum number of variables is given by the total number of integration points in the mesh. The optimum random field discretization for a given finite element mesh is therefore a discretization relative to the integration points and a series of methods has been proposed for this purpose (Sudret and Der Kiureghian, 2000).

Here, a finite element is subdivided into cells, each of which contains an integration point (Figure 1). The integration point is assigned the cell average of the underlying random field. This way of discretization of the random field is consistent with local averaging theory (Vanmarcke, 1983) in taking account of the variance reduction as a result of spatial averaging. With $\bar{z}$ being the cell average of random field values $z(\vec{x})$, the exact solution of the variance reduction factor $\gamma = \mathrm{E}[\bar{z}^2]/\mathrm{E}[z^2]$ is found by

$$\gamma = \frac{1}{V^2} \int_{\vec{x}_i \in \Omega} \int_{\vec{x}_j \in \Omega} \rho(\vec{x}_i - \vec{x}_j) dV dV \tag{4}$$

where $\rho(\vec{x}_i - \vec{x}_j)$ is the spatial correlation function of the underlying random field. The analytical expression (4) is approximated by Gauss-Legendre quadrature, in which the order of the quadrature determines the accuracy of the variance reduction to be accounted for. In equivalence with (4), the correlation between any two discretized cells $A$ and $B$ can be found as the double integral over their domains $\Omega_A$ and $\Omega_B$:

$$\rho(\Omega_A, \Omega_B) = \frac{1}{V_A V_B} \int_{\Omega_A} \int_{\Omega_B} \rho(\vec{x}_B - \vec{x}_A) dV dV \tag{5}$$

Given a discretization $\boldsymbol{Z}$ of the random field by means of $n$ cells, the $n \times n$ autocovariance matrix $\mathbf{C}$ is defined as the expected covariance between any two components of $\boldsymbol{Z}$. With standard deviation $\sigma_Z = 1$, $\mathbf{C}$ can be directly calculated from (5) so that

$$\mathbf{C} = \mathrm{E}[\boldsymbol{Z}\boldsymbol{Z}^\intercal] \tag{6}$$

Covariance matrix decomposition (CMD) for random field generation makes use of the orthogonality of decomposed matrices to characterize the random field as the product of an orthogonal set of $n$ vectors and a set of $n$ uncorrelated random numbers. With $\mathbf{A}$ being a $n \times n$ matrix containing the $n$ orthogonal vectors, the random field $\boldsymbol{Z}$ is defined as

$$\boldsymbol{Z} = \mathbf{A}\boldsymbol{\xi} \tag{7}$$

where $\boldsymbol{\xi}$ is an $n$-dimensional vector of uncorrelated standard normal random numbers to be drawn from a standard normal sampling space. From (6) and (7) it follows that:

$$\mathrm{E}[\boldsymbol{Z}\boldsymbol{Z}^\intercal] = \mathrm{E}[\mathbf{A}\boldsymbol{\xi}(\mathbf{A}\boldsymbol{\xi})^\intercal] = \mathrm{E}[\mathbf{A}\boldsymbol{\xi}\boldsymbol{\xi}^\intercal\mathbf{A}^\intercal] = \mathbf{A}\mathbf{A}^\intercal = \mathbf{C} \tag{8}$$

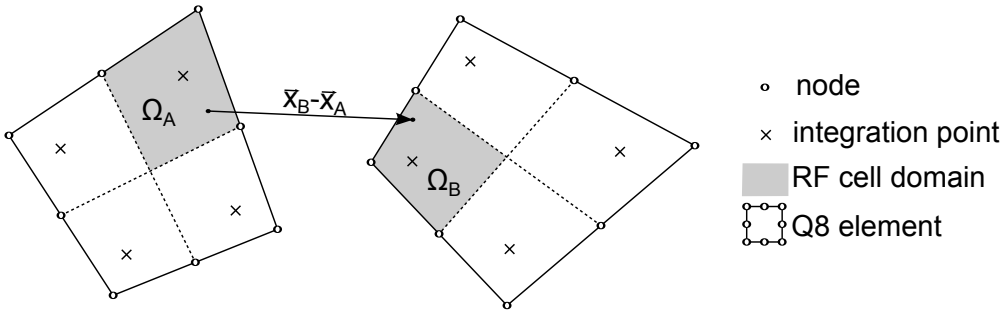


Figure 1: RF discretization by RF cell domains as finite element quadrants

From this relation it follows that $\mathbf{A}$ is a decomposition of covariance matrix $\mathbf{C}$. As covariance matrices are generally positive definite, Cholesky decomposition $\mathbf{C} = \mathbf{L}\mathbf{L}^\intercal$ is a possible method of decomposition. However, in the case of strongly correlated cells, Cholesky decomposition is prone to numerical instabilities and additional measures are needed for decomposing the covariance matrix (Green et al., 2015). Other methods are based on eigen-decomposition of the covariance matrix, as is the case in Karhunen-Loève decomposition (Huang et al., 2001). If the random field is discretized by $n$ cells, the matrix of $n$ orthonormal eigenvectors $\mathbf{\Phi}$ and the diagonal matrix of $n$ eigenvalues $\mathbf{\Lambda}$ characterize the $n \times n$ covariance matrix $\mathbf{C}$ exactly. In this case, eigenvectors and eigenvalues are defined such that

$$\mathbf{C} = \mathbf{\Phi}\mathbf{\Lambda}\mathbf{\Phi}^\intercal \tag{9}$$

The discretized random field $\boldsymbol{Z}$ can now be defined either as

$$\boldsymbol{Z} = \mathbf{\Phi}\mathbf{\Lambda}^{1/2}\mathbf{\Phi}^\intercal\boldsymbol{\xi} \tag{10}$$

or

$$\boldsymbol{Z} = \mathbf{\Phi}\mathbf{\Lambda}^{1/2}\boldsymbol{\xi} \tag{11}$$

where both satisfy the covariance condition of (6), in which $\mathbf{C}$ accounts for the variance reduction due to local averaging according to (5).

Numerical methods generally have to be used to derive the decomposition with the dimensions of the matrix to be decomposed equal to the number of discretization cells $n$. It is clear that the decomposition of the random field into either a Cholesky lower triangle $\mathbf{L}$ or eigenvectors/eigenvalues becomes computationally expensive for large numbers of discretization cells in the general case of unstructured discretization meshes. However, more efficient methods (e.g. EOLE (Li and Der Kiureghian, 1993) and LAS (Fenton and Vanmarcke, 1990)), will necessarily include restrictions in accuracy or detail of the variability of the fields.

## 4. Subset simulation

Subset simulation (Au and Beck, 2001; Au and Wang, 2014) is a method to simulate events with small probabilities in the framework of MCS by restricting the analysis to a subset $\Omega^{(i)}$ of the total sampling space $\Omega^{(0)}$. A series of subsets can be defined to subsequently narrow down the represented domain of the sampling space such that $\Omega^{(i)} \subset \Omega^{(i-1)}$ with subset $i = 1, 2, ..., m$.

The probability of occurrence $\mathrm{P}(F^{(i)})$ of an event $F^{(i)}$ from a subspace $\Omega^{(i)}$ can be written as

$$\mathrm{P}(F^{(i)}) = \mathrm{P}(F^{(i)}|F^{(i-1)})\mathrm{P}(F^{(i-1)}) \tag{12}$$

With the set of events $\Omega^{(0)}$ having the corresponding probability $\mathrm{P}(F^{(0)}) = 1$, the probability of an event at subset level ($m$) taking place is given by the product of conditional probabilities of the subsets:

$$\mathrm{P}(F^{(m)}) = \prod_{i=1}^{m} \mathrm{P}(F^{(i)}|F^{(i-1)}) \tag{13}$$

Subset simulation requires additional realizations to be generated for a sufficiently detailed sampling of each subset under consideration. This requires sampling from the unknown conditional distribution function (the posterior distribution) and relies on the Metropolis algorithm (Metropolis et al., 1953) and its derivatives. In combination with Markov chain Monte Carlo (MCMC) simulation, these algorithms aim at unbiased sampling in the conditional sampling space, without prior knowledge of the conditional probability density function. The Modified Metropolis algorithm (MMA) was proposed by Au and Beck (2001) to increase the efficiency of sampling from the unknown posterior distribution in multidimensional sampling space. This modification made it possible to apply subset simulation in high-dimensional problems such as RFEM.

Applications of subset simulation to high-dimensional problems in geotechnical engineering are found in foundation engineering (Ahmed and Soubra, 2012), rock slope stability (Jiang et al., 2017) and soil slope stability based on limit equilibrium or finite element methods (Wang et al., 2011; Jiang and Huang, 2016; Li et al., 2016a,b; Xiao et al., 2016; Huang et al., 2016). Several additional improvements of the MMA were subsequently proposed to increase the efficiency of the algorithm; for example, see Papaioannou et al. (2015) for a comparison of several of these methods. Other optimized versions are designed to reduce the number of individual Markov chains in MCMC simulation techniques.

This paper focuses on the original version of the MMA (Au and Beck, 2001) and its use for the simulation of rare events in slope stability analysis using the random finite element method. To avoid confusion between different versions of the MMA algorithm, it is repeated here. Given a link $j > 1$ in Markov chain $k$ with samples from the conditional sampling space $\Omega^{(i)}$ as a subspace from sampling space $\Omega^{(0)}$ with standard normal prior distribution $q^{(0)}$, a realization $\boldsymbol{\theta}^{(i)}_{(k,j)}$ is generated from seed $\boldsymbol{\theta}^{(i)}_{(k,j-1)}$ as follows:

1. Take the preceding step in the Markov chain as seed $\boldsymbol{\theta}^s = \boldsymbol{\theta}^{(i)}_{(k,j-1)}$
2. Generate proposal state $\boldsymbol{\theta}^p$: components $\theta^p_i$ are generated from the proposal distribution $p(\theta^p_i|\theta^s_i) = \theta^s_i + \xi^{Ms}_i$
3. Ratio $r_i = q_i(\theta^p_i)/q(\theta^s_i)$ is used to accept/reject component-wise against uniform random number $\xi^{01}$,

$$\theta^p_i = \theta^s_i \quad \text{if} \quad \xi^{01}_i >= r_i \tag{14}$$

$$\theta^p_i = \theta^p_i \quad \text{if} \quad \xi^{01}_i < r_i \tag{15}$$

4. The updated proposal state $\boldsymbol{\theta}^p$ is checked to be part of $\Omega^{(i)}$ (i.e. $I^{(i)}(\boldsymbol{\theta}^p) = 1$),

$$\boldsymbol{\theta}^{(i)}_{(k,j)} = \boldsymbol{\theta}^p \qquad \text{if} \quad I^{(i)}(\boldsymbol{\theta}^p) = 1 \tag{16}$$

$$\boldsymbol{\theta}^{(i)}_{(k,j)} = \boldsymbol{\theta}^s \qquad \text{if} \quad I^{(i)}(\boldsymbol{\theta}^p) = 0 \tag{17}$$

In this algorithm, $\boldsymbol{\xi}^{Ms}$ is a column vector of zero-mean, non-skewed random numbers, characterizing the Markov step in sampling space. $\xi^{01}_i$ is a random number with a uniform distribution between 0 and 1, $q(.)$ is the unconditional marginal (prior) distribution, which is standard normal, and $I^{(i)}(\boldsymbol{\theta})$ is an indicator of the performance function. Note that the final step is an acceptance/rejection of the proposal state. The proposal state is rejected when it is not part of subset $(i)$, in which case the seed is used to take the place of the proposal state. This implies that the rejection of proposal states leads to identical realizations within the Markov chain. The acceptance rate of proposal states is influenced by the size of the Markov steps ($\boldsymbol{\xi}^{Ms}$). Small Markov steps lead to high acceptance rates but also to high correlations between subsequent steps in the Markov chain, thereby leading to an inefficient sampling of the subset. The key to an efficient MMA is to have a high acceptance rate in combination with large Markov steps to minimize the correlation between realizations in the chain. The efficiency is highly dependent on the type of problem (i.e. the deterministic function) and optimization of MCMC simulations would certainly require adaptive algorithms.

### *4.1. Standard subset simulation in slope reliability analysis*

The use of subset simulations in slope stability analysis using RFEM allows the simulation of failure events with small probabilities. These small probabilities would typically be the subset of realizations of a crude Monte Carlo simulation that have $FOS \leq 1.0$. Depending on the reliability distribution, these probabilities can be very small (say $p_f = 1.0 \times 10^{-6}$) and generating these realizations by crude MCS would require many realizations ($N >> 1 \times 10^6$). Subset simulation is used to generate subsets of realizations that have a $FOS$ smaller than intermediate levels of

strength reduction factors $f_s^{(i)}$. From a subset $(i)$ with $N_t$ realizations, the next subset $(i+1)$ is defined as $FOS < f_s^{(i+1)}$ based on the $N_c = p_0 N_t$ weakest realizations in subset $(i)$, with $p_0 = \mathrm{P}(F^{(i+1)}|F^{(i)})$ being the conditional probability between subsets as a simulation input parameter. MCMC using MMA is then used to generate more realizations in the newly defined subset and the process is repeated until the desired level of strength reduction is reached. The choice of simulation input parameters $N_t$ and $p_0$ defines the exact number of simulations per subset and the rate at which the probability level decreases per subset.

The method requires the results of the $N_t$ realizations to be sorted based on their $FOS$, so as to provide a means of selecting the weakest $N_c$. This means that the full SSR method has to be applied, which makes the computational cost high with respect to applying MCS-DSA directly at the $f_s$ under consideration.

Li et al. (2016a) proposed to use subset simulations in combination with limit equilibrium methods (LEM) to generate subsets of realizations of slope stabilities at different levels of probability and analyze a reduced number of samples from the generated subsets using FEM for establishing the actual $FOS$. This way of circumventing the tedious task of evaluating all realizations led to an impressive reduction in the computational cost. However, a rigorous demonstration of ergodicity with RFEM was not demonstrated and the method hinges on the unbiased correlation between LEM and FEM, which might not hold with respect to failure mechanisms. A similar approach to reduce the computational cost of 3D slope stability analysis was followed by Xiao et al. (2016) who evaluated 3D surrogate models with coarse meshes in a preliminary subset simulation, after which a detailed finite element analysis was made on a selection of the preliminary realizations.

Huang et al. (2016) recently proposed a form of subset selection in which the amount of yielding was used as a relative indicator of the factor of safety to sort realizations. The accuracy of the calculated probability of failure was verified against MCS and subset simulation with subset selection based on SSR. However, in the authors view, an approach with subset threshold selection based on performance indicators could lead to a bias with respect to modes of failure in certain cases. When an indicator is not a monotonic function of the factor of safety, subset selection will over-sample realizations with this indicator. As a result, any performance characteristic positively correlated to the indicator will be over-sampled in the subset selection and negatively correlated characteristics will be under-sampled. This could lead to a bias in the results which does not disappear with increasing subset sample sizes. In detailed studies of modes of failure, any indicator that is not a monotonic function of the factor of safety should preferably be avoided for this reason.

### *4.2. Modification of subset simulation*

To overcome the necessity of performing SSR for each realization, a modification is proposed here to replace the SSR method in the subset simulation with a direct stability analysis (DSA) against a given $f_s$. The concept of the proposed modification is to change from the usual probability-based subset selection (based on subset conditional probability $p_0 = \mathrm{P}(F^{(i+1)}|F^{(i)})$) to a condition-based subset selection (based on $f_s^{(i+1)}$). This modification avoids the ranking of realizations for selecting the seeds of the next subsets, so that the exact $FOS$ of the slope is not needed in the analysis. Only the acceptance to the next subset is used for seed selection, thereby reducing the required computation from SSR to DSA.

Figure 2 graphically represents the proposed approach:

- Strength reduction thresholds $f_s^{(1)}$ and $f_s^{(2)}$ are initiated, after which MCS-DSA is started against $f_s^{(1)}$ until $N_c$ failure events ($F^{(1)}$) are observed in a total of $N_t^{(0)}$ realizations. The first intermediate probability of failure is found as $p_f^{(1)} = N_c/N_t^{(0)}$. Realizations leading to $F^{(1)}$ are selected as the seeds for the first subset (Figure 2a).
- MCMC starting from the seeds of the first subset is used to generate new realizations in the first subset (all having $F^{(1)}$) and tested by DSA at $f_s^{(2)}$ for failure events $F^{(2)}$ until $N_c$ failure events $F^{(2)}$ are observed in a total of $N_t^{(1)}$ realizations. The second intermediate probability of failure is found as $p_f^{(2)} = N_c/N_t^{(1)} p_f^{(1)}$ and realizations leading to $F^{(2)}$ are selected as seeds for the next subset (Figure 2b).
- A theoretical probability distribution is fitted through the two available points $p_f(f_s^{(1)})$ and $p_f(f_s^{(2)})$, based on which the next threshold factor $f_s^{(3)}$ is defined corresponding to the next target probability $p_0 p_f^{(2)}$ (Figure 2c).
- MCMC simulations are repeated, starting from the new seeds to generate $N_t^{(2)}$ realizations with $N_c$ events $F^{(3)}$. The next intermediate probability of failure is found as $p_f^{(3)} = N_c/N_t^{(2)} p_f^{(2)}$, with $N_c/N_t^{(2)} \approx p_0$ (Figure 2d).

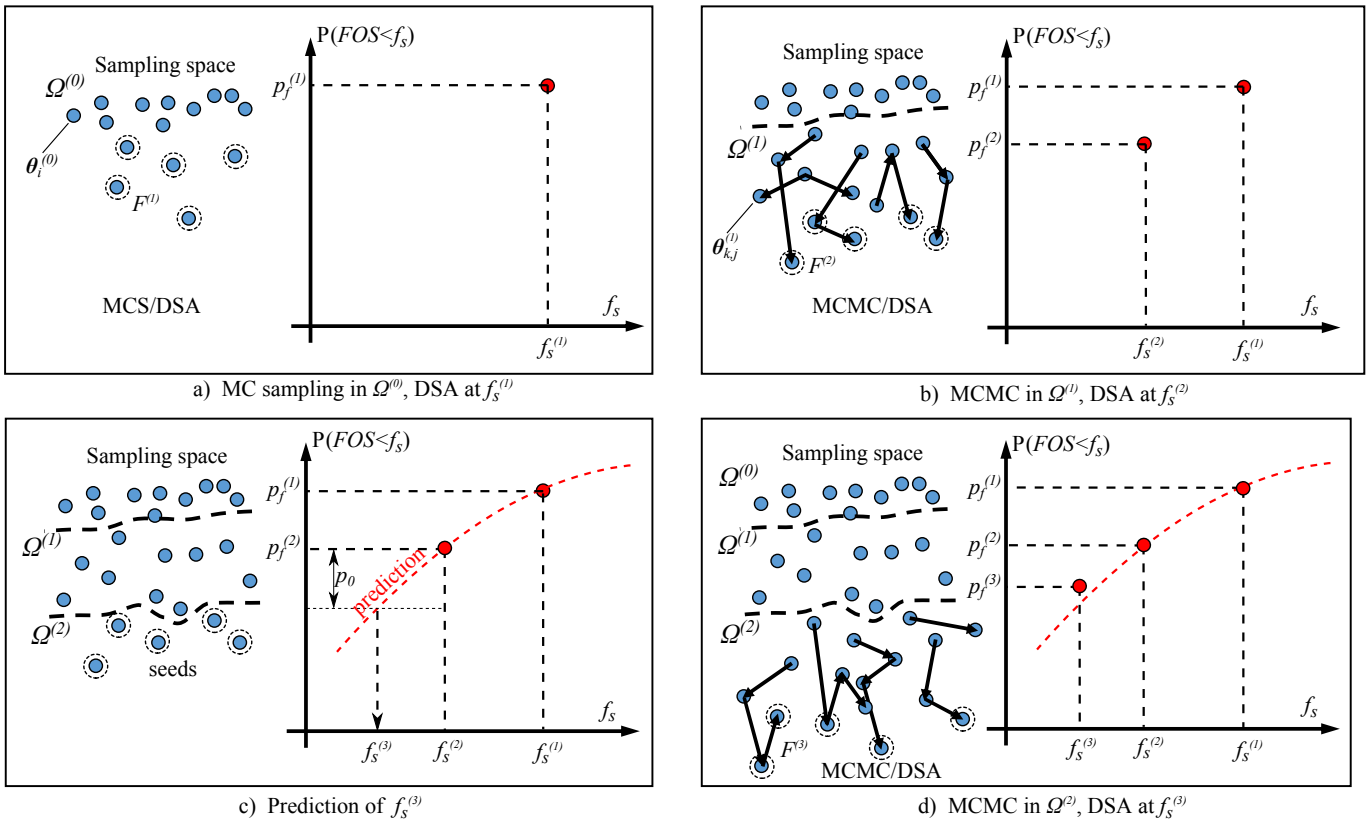


a) MC sampling in $\Omega^{(0)}$, DSA at $f_s^{(1)}$

b) MCMC in $\Omega^{(1)}$, DSA at $f_s^{(2)}$

c) Prediction of $f_s^{(3)}$

d) MCMC in $\Omega^{(2)}$, DSA at $f_s^{(3)}$

Figure 2: Schematic representation of proposed scheme for subset simulation. (Modified after Li et al. (2016b))

- Again, the next intermediate threshold factor $f_s^{(4)}$ is predicted based on the latest two data points $p_f(f_s^{(2)})$ and $p_f(f_s^{(3)})$, after which MCMC is repeated to generate the realizations for subset 3, tested in DSA against $f_s^{(4)}$ until $N_c$ failure events $F^{(4)}$ are found. This routine is repeated for subsequent subsets until the strength reduction factor is at the desired level (in this case $f_s = 1.00$).

The target conditional subset probability $p_0$ and number of conditional realizations $N_c$ (i.e. number of seeds per subset) are user-defined simulation parameters. Furthermore, initiation thresholds $f_s^{(1)}$ and $f_s^{(2)}$ need to be chosen so that $p_f^{(1)} \approx p_0$ and $p_f^{(2)} \approx p_0^2$. The total number of realizations per subset $N_t^{(i)}$, as well as the total number of subsets needed to reach the target strength reduction factor $f_s^{end}$, depends on the correct prediction of conditional subset probabilities. Following Equation (12), the final probability of failure is computed as:

$$p_f = \prod_{i=1}^{m} \frac{N_c}{N_t^{(i)}} \tag{18}$$

The code is summarized in the algorithmic scheme of Figure 3.

The target conditional probability $p_0$, used to determine the intermediate strength reduction factors $f_s^{(i+2)}$, indirectly sets the expected number of steps per Markov chain to $1/p_0 - 1$ per subset. An optimum value for $p_0$ is difficult to define, as it depends on the efficiency of the Markov chains in covering the conditional sampling space. A theoretical optimum can therefore not be derived. A value of $p_0 = 0.1$ is used here, as was suggested by Au and Beck (2001) for efficient subset simulation and used in most applications of the method (Li et al., 2016a,b; Huang et al., 2016). However, due to the estimation of subsequent intermediate strength reduction factors, the actual conditional probability of failure can be different from the envisioned value. This only has an effect on the efficiency of the method and does not influence the accuracy.

1. choose $f_s^{(1)}$ and $f_s^{(2)}$;
2. generate unconditional realizations $\boldsymbol{\theta}_i^{(0)}$ to form set $\{\boldsymbol{\theta}^{(0)}\}$. Check for $F^{(1)}(\boldsymbol{\theta}_i^{(0)})$ until $\sum \boldsymbol{I}^{(0)} = N_c$;
3. select conditional subset $\{\boldsymbol{\theta}_{(k,1)}^{(1)}\} = \{\boldsymbol{\theta}^{(0)}|F^{(1)}\}$ containing all failed realizations;
4. $i = 1$;
5. expand $\{\boldsymbol{\theta}^{(i)}\}$ using MCMC and check for $F^{(i+1)}$ until $\sum \boldsymbol{I}^{(i+1)} = N_c$ ;
6. select conditional subset as next seeds $\{\boldsymbol{\theta}_{(k,1)}^{(i+1)}\} = \{\boldsymbol{\theta}^{(i)}|F^{(i+1)}\}$;
7. determine $p_f^{(i+1)} = p_f^{(i)} N_c / N_t^{(i)}$;
8. predict $f_s^{(i+2)} \geq f_s^{end}$ (section 4.3);
9. $i = i + 1$;
10. if $f_s^{(i+1)} \neq f_s^{end}$ goto 5;
11. end of SS with $\{\boldsymbol{\theta}^{(i)}\}$ being the resulting subset with $FOS < f_s^{end}$

Figure 3: Modified subset simulation algorithm

### *4.3. Prediction of the intermediate threshold $f_s^{(i+2)}$*

The seeds for the next subset are selected based on the prediction of the next threshold factor of safety $f_s^{(i+2)}$ and testing the realizations of the current subset against it. The next point $f_s^{(i+2)}$ is the intercept of a fitted probability distribution function (PDF) and the line $p_f = p_0 p_f^{(i+1)}$, with $p_0$ being the target conditional probability as the ideal probability gain per subset $\mathrm{P}(F^{(i+2)}|F^{(i+1)})$. Because the fitting PDF only approximates the actual PDF and the points for fitting contain an uncertainty relative to the uncertainty in the conditional probability of failure per subset, the ideal conditional probability $p_0$ can only be approximated. However, because the subset ensemble size is based on the total number of failed realizations, this is corrected for in the algorithm and only the efficiency of the method is influenced. Only very irregular probability density functions will lead to problems, when the actual conditional probability $P(F^{(i+2)}|F^{(i+1)})$ is much smaller than the target probability $p_0$ that was used to set $f_s^{(i+2)}$. In the case of such irregular probability density functions, discussed in more detail in Au and Wang (2014), additional corrections of the subset threshold might be considered to avoid conditional probabilities far from the target probability.

Different strategies can be considered to predict the most efficient level of $f_s^{(i+2)}$ based on the $p_f(f_s)$ points determined so far, e.g. regression of a PDF or a polynomial fit constrained by theoretical limits such as monotonic increase of $p_f(f_s)$. Another strategy is to make a prediction based on a local fit, in an attempt to better account for possible local variations of the probability distribution. This is done here, by fitting a theoretical PDF to the latest two points, $p_f(f_s^{(i)})$ and $p_f(f_s^{(i+1)})$, to predict $f_s^{(i+2)}$. Different choices for the fitting PDF can be made. The most straightforward is a linear extrapolation in the $f_s - \log(p_f)$ plane, although this method was found to strongly overestimate the step size, resulting in excessive numbers of realizations per subset and a reduction in the global efficiency.

In this work, a more conservative estimation (with respect to the step size in the intermediate factor of safety $f_s^{(i+1)} - f_s^{(i+2)}$) is used by fitting a lognormal distribution. This first requires estimations $\hat{\mu}_f$ and $\hat{\sigma}_f$ of the lognormal distribution parameters $\mu_{LN}$ and $\sigma_{LN}$, from which $f_s^{(i+2)}$ can be determined at the desired level of probability $p_0 p_f^{(i+1)}$:

$$\hat{\sigma}_f = \frac{\ln(f_s^{(i)}/f_s^{(i+1)})}{Z^{(i)} - Z^{(i+1)}} \tag{19}$$

$$\hat{\mu}_f = \ln\left(f_s^{(i+1)}\right) - \hat{\sigma}_f Z^{(i+1)}\Big) \tag{20}$$

$$f_s^{(i+2)} = \exp\left(\hat{\mu}_f + \hat{\sigma}_f \Phi^{-1}\left(p_0 p_f^{(i+1)}\right)\right) \tag{21}$$

where function $\Phi(.)$ is the standard normal PDF and $Z^{(i)}$ is the standard score of probability $p_f^{(i)}$.

To initiate the simulation, the first two strength reduction factors, $f_s^{(1)}$ and $f_s^{(2)}$, need to be selected. A good starting point would be the estimations of $f_s$ corresponding to probabilities $p_f^{(1)} = 0.1$ and $p_f^{(2)} = 0.01$, but any other estimation

(e.g. higher strength reduction factors) will also work under the condition that $p_f = 1$ is avoided. This selection requires some prior knowledge of the probability function for the method to achieve optimal efficiency, which can be based on a limited number of simulations used to explore the probability function, or on user experience based on the factor of safety of homogeneous slopes and the coefficient of variation in the strength parameters. In the following, the chosen initial values are $f_s^{(1)} = 1.5$ and $f_s^{(2)} = 1.4$. These values have not been optimised with respect to the efficiency of the method, as will be discussed in Section 6.

As soon as the predicted strength reduction factor $f_s^{(i+2)}$ passes below the target level $f_s^{end}$, it is corrected to match the target value, i.e. $f_s^{(i+2)} = f_s^{end}$. This correction sets the final subset level $m = i+2$ to be considered in the simulation. Note that, due to the correction of the final level of $f_s$, the conditional probability of the final subset is generally larger than $p_0$. To avoid subsets with conditional probabilities close to 1 and optimize efficiency, an additional approach can be to also correct predicted threshold values $f_s^{(i+2)}$ to $f_s^{end}$ when they are slightly larger than $f_s^{end}$.

### *4.4. Assessment of efficiency*

The coefficient of variation $\delta$ of the estimation of a probability $p$ determined from $N$ independent realizations is derived from the Bernouilli distribution as:

$$\delta = \frac{\mathrm{E}[p]}{\sqrt{\mathrm{E}[p^2]}} = \sqrt{\frac{1-p}{pN}} \tag{22}$$

Since the realizations in subset simulation are generated in Markov chains using the MMA, they suffer from a correlation inside the chain. This correlation depends on the Markov step size and the MMA acceptance ratio: small Markov steps generate similar realizations whereas rejection of proposal realizations results in duplication of the seed. Both lead to correlation between realizations within the seeds and the coefficient of variation $\delta^{(i)}$ of individual levels $i > 1$ during subset simulation needs to be corrected for this correlation. Au and Beck (2001) derived a correlation factor $\gamma_k$ to correct for the in-chain dependency:

$$\delta^{(i)} = \sqrt{\frac{1-p^{(i)}}{p^{(i)}N_t^{(i)}}(1+\gamma^{(i)})} \tag{23}$$

where $N_t^{(i)}$ is the total number of realizations at the current subset level. The correlation term $\gamma^{(i)}$ is derived as

$$\gamma^{(i)} = 2\sum_{k=1}^{K^{(i)}} \frac{N_t^{(i)} - kN_c}{N_t^{(i)}} \frac{R^{(i)}(k)}{R^{(i)}(0)} \tag{24}$$

where $N_t^{(i)} - kN_c$ is the number of times a pair of realizations is at a distance of $k$ steps in the Markov chain and $K^{(i)}$ is the maximum number of steps taken in any of the Markov chains in subset $(i)$. $R^{(i)}(k)$ is the covariance between realizations at a distance of $k$ steps in the Markov chain and $R^{(i)}(0)$ is the variance of the indicator $\boldsymbol{I}^{(i)}$, here written with components $I_{jl}^{(i)}$ for the realization of step $l$ in chain $j$. The covariance sequence $R^{(i)}(k)$ can be estimated as

$$R^{(i)}(k) \approx \hat{R}^{(i)}(k) = \frac{1}{N_t^{(i)} - kN_c} \sum_{j=1}^{N_c} \sum_{l=1}^{L_j^{(i)}-k} I_{jl}^{(i)} I_{j,l+k}^{(i)} - \left(\frac{N_c}{N_t^{(i)}}\right)^2 \tag{25}$$

where $L_j^{(i)}$ is the number of steps of Markov chain $j$ in subset $(i)$, which is equal to $K^{(i)}$ or $K^{(i)} - 1$.

Not only can the correlation in subsequent steps of the Markov chain influence the independence of the realizations, but also the correlation between the seeds of each subset has its influence on the efficiency of upcoming subsets. Although it has been suggested that the correlation between seeds can be neglected (Au and Beck, 2001; Li et al., 2016b), the results in Section 6.1 will demonstrate that there is indeed an influence of correlation between seeds and that ignoring this influence will lead to an underestimation of the coefficient of variation in the estimation of $p_f$. Assuming that the seeds for each subset are independent, a lower bound of the coefficient of variation $\delta_L$ can be

formulated under the assumption that the probabilities of failure in subsequent levels of subsets are fully independent (Au and Beck, 2001):

$$\delta_L^2 = \sum_{i=1}^{m} {\delta^{(i)}}^2 + O(N^{-1}) \tag{26}$$

The upper bound can be given for fully correlated seeds as (Au and Beck, 2001):

$$\delta_U^2 = \sum_{i,j=1}^{m} \delta^{(i)}\delta^{(j)} + O(N^{-1}) \tag{27}$$

A more reliable estimation of the coefficient of variation of a single subset simulation would require information on the acceptance ratio and its link with generated samples that lead to failure events in the subsequent subset. As a result, multiple simulations will be required to determine the effective coefficient of variation of the estimation of the probability of failure, independent of any assumptions on the conditions under which realizations will survive in the next subset.

## 5. Slope stability analysis at small probabilities of failure

The probability of failure of an idealised slope is investigated. The slope is of 5 m height, inclined at an angle of 45°, and considered to be constructed of a cohesive soil (no frictional component) with varying undrained shear strength $c_u$ following a lognormal distribution with a mean of 32 kPa and a standard deviation of 8 kPa. The spatial variation of $c_u$ is assumed to be characterized by a horizontal scale of fluctuation of $\theta_1 = 8$ m, a vertical scale of fluctuation of $\theta_2 = 1.25$ m and a Markov spatial correlation function for normalized length scale $\tau$:

$$\rho(\tau) = \exp(-2\tau) \qquad \tau = \sqrt{\left(\frac{\Delta x_1}{\theta_1}\right)^2 + \left(\frac{\Delta x_2}{\theta_2}\right)^2} \tag{28}$$

Random fields are generated using CMD as described in Section 3. Figure 4 shows the problem geometry and a typical random field realization of the spatial variability of $c_u$. Displacements are constrained on the lower domain boundary, whereas only horizontal displacement is constrained on left and right boundaries.

### *5.1. Monte Carlo simulations with Shear Strength Reduction (MCS-SSR)*

As a reference case, a Monte Carlo simulation using SSR on $2 \times 10^4$ independent realizations is performed. The iterative precision of the lowest strength reduction factor leading to failure is $1 \times 10^{-3}$. The cumulative distribution function of the strength reduction factor to induce slope failure is given in Figure 5. Note that these strength reduction factors are the result of an analysis by SSR, which means that they are equal to $FOS$.

### *5.2. Monte Carlo simulations with Direct Stability Analysis of slope stability (MCS-DSA)*

Direct stability analysis of the slope stability is performed at strength reduction factors of $f_s = 1.2$, $f_s = 1.3$ and $f_s = 1.4$ for sample sizes of 20,000 realizations each. The resulting probabilities of failure for each simulation are included in Figure 5. Note that the accuracy in the prediction is as high as obtained with the SSR method according to (22).

### *5.3. Subset simulation probability simulations (100×)*

Subset simulations are performed on the same problem, to evaluate the probability of failure at $f_s = 1.3 - 1.2 - 1.1 - 1.0$. The number of realizations per subset was controlled by the conditional subset number $N_c = 200$. The target conditional subset probability $p_0 = 0.1$ was taken as the proposed value for $p_0$ in the original subset simulation algorithm by Au and Beck (2001). To assess the reliability of the predictions of the subset simulation, each simulation is repeated 100 times. The coefficient of variation in the predicted failure probabilities can be estimated from the spread in the outcomes of these 100 simulations. Figure 6 contains the results of all 100 simulations for the 4 cases, together with

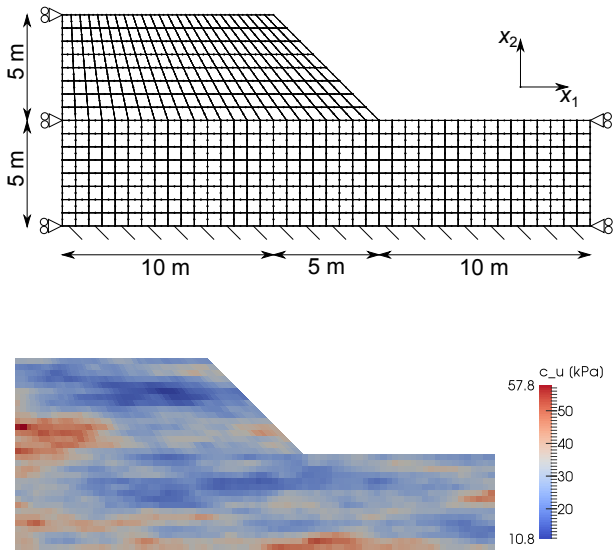


Figure 4: Finite element mesh with boundary conditions and typical realization of $c_u$, distributed lognormally with mean $\mu = 32$ kPa, standard deviation $\sigma = 8$ kPa, $\theta_1 = 8.0$ m, $\theta_2 = 1.25$ m

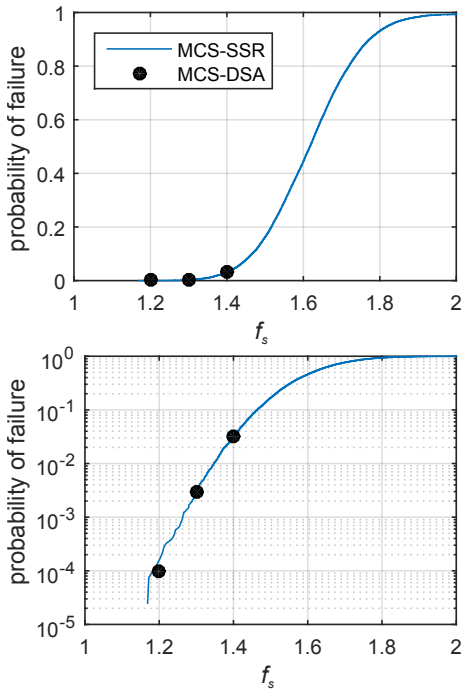


Figure 5: Cumulative distribution function of the smallest strength reduction factor leading to failure, obtained by MCS-SSR and MCS-DSA over 20,000 realizations.

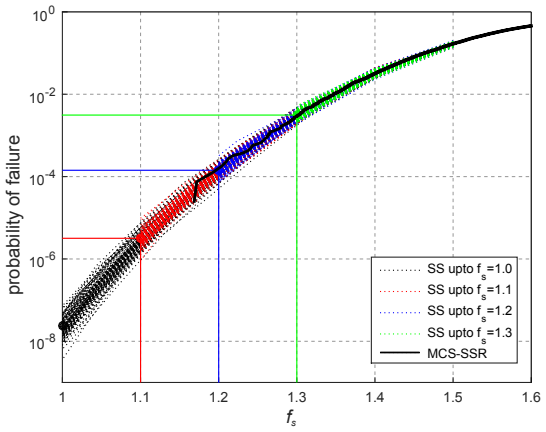


Figure 6: Probability of $FOS < f_s$ obtained by 100 subset simulations with $N_c = 200$. MCS-SSR results contains an evaluation of 20,000 realizations.

| | $\hat{p}_f$ | $CoV$ |
|---|---|---|
| SS | $1.403 \times 10^{-4}$ | 0.029 |
| MCS | $1.430 \times 10^{-4}$ | 0.026 |

Table 1: Estimated probability of failure $\hat{p}_f$ at $f_s = 1.2$ using subset simulation (SS) and Monte Carlo simulation (MCS).

the reference simulation from Figure 5. Each line represents the calculated probability of failure of a single simulation as a function of the intermediate threshold strength reduction factor until the final strength reduction factor.

A first verification of subset simulation is based on the computed probability of failure $\hat{p}_f$ at $f_s = 1.2$ as presented in Figure 6. From 100 subset simulations with $N_c = 200$, the estimated probability of failure $\hat{p}_f^{SS}$ and its coefficient of variation $CoV^{SS}$ are computed. MCS using DSA with $10^7$ realizations is performed as a reference, resulting in an estimated probability of failure $\hat{p}^{MCS}$ with corresponding coefficient of variation according to (22). The resulting calculated probabilities $\hat{p}_f$ are given in Table 1, together with the coefficient of variation to characterize confidence in the outcome. The relative difference between $\hat{p}_f^{SS}$ and $\hat{p}_f^{MCS}$ is smaller than the coefficients of variation and the results can therefore be considered consistent. This demonstrates that subset simulation does indeed, from a practical point of view, give an unbiased estimation of the probability of failure compared to MCS for the considered type of application.

Note that the original version of subset simulation is considered to be asymptotically unbiased and ergodic for increasing numbers of realizations $N$ (Au and Wang, 2014). With the proposed method of performance-based subset selection only influencing the conditional probability $\mathrm{P}(F^{(i)}|F^{(i-1)})$, these properties of subset simulation are therefore considered to be maintained.

## 6. Evaluation of simulation efficiency

### *6.1. Algorithmic efficiency*

The efficiency of subset simulation as a function of the target strength reduction factor is investigated. A series of subset simulations is repeated 100 times for each target $f_s$, using $N_c = 200$ conditional realizations per subset and initial factors $f_s^{(1)} = 1.5$ and $f_s^{(2)} = 1.4$. The expected probability of failure is estimated over the 100 realizations as well as the coefficient of variation $CoV$ between the results of the individual simulations. This coefficient of variation can be normalized against the number of FEM calls in a simulation as $CoV_n = CoV\sqrt{N}$, to quantify the relative efficiency. The equivalent coefficient of variation $CoV_n^{MCS}$ that would have been obtained in MCS for the same level

| $f_s$ | $p_f$ | $CoV^{ss}$ | $CoV_n^{ss}$ | $\mathrm{CoV}_n^{MCS}$ | alg. eff. |
|---|---|---|---|---|---|
| 1.50 | $1.67 \times 10^{-1}$ | 0.065* | 2.23* | 2.23* | 1.0* |
| 1.40 | $3.23 \times 10^{-2}$ | 0.117 | 6.11 | 5.47* | 0.82 |
| 1.30 | $3.11 \times 10^{-3}$ | 0.204 | 14.8 | 17.9* | 1.5 |
| 1.25 | $7.07 \times 10^{-4}$ | 0.265 | 21.4 | 37.6* | 3.1 |
| 1.20 | $1.39 \times 10^{-4}$ | 0.290 | 26.1 | 84.8* | 11 |
| 1.10 | $3.22 \times 10^{-6}$ | 0.430 | 47.1 | 557* | 140 |
| 1.00 | $2.40 \times 10^{-8}$ | 0.560 | 72.9 | 6450* | 7823 |

Table 2: Performance analysis of subset simulations based on 100 simulations with $N_c = 200$, including relative algorithmic efficiency. [*]=theoretical value based on probability of failure $p_f$.

of probability is given by:

$$CoV_n^{MCS} = \sqrt{\frac{1 - p_f}{p_f}} \tag{29}$$

Table 2 lists the final strength reduction factors in the simulations and corresponding results. For $f_s^{end} = 1.5$, SS does not continue beyond the initiation stage and is therefore identical to MCS and the efficiency is the same for both methods. Subset simulation is found to be less efficient at $f_s^{end} = 1.4$, which happens to be equal to $f_s^{(2)}$. The relative efficiency of SS increases with decreasing probabilities, as can be seen from Figure 7; the relative difference in normalized coefficient of variation for SS and MCS gets larger with decreasing failure probability level. As the normalized coefficient of variation $CoV_n$ can be translated into relative numbers of simulations, the relative efficiency of SS can be computed as $(CoV_n^{MCS}/CoV_n^{SS})^2$, expressed in the relative number of calls to the deterministic function (i.e., the FEM computation for DSA). Figure 8 shows that the relative efficiency based on the number of FEM calls becomes larger than 1 for $p_f < 0.01$ and increases to several orders of magnitude for smaller probabilities. The lower efficiency of SS at larger probability is due to the non-optimal initiation of SS (i.e., the choice of $f_s^{(1)}$ and $f_s^{(2)}$).

Upper and lower bounds of the normalized coefficient of variation, computed by (26)-(27), are included in Figures 7 and 8. The subset coefficients of variation $\delta^{(i)}$ are computed for the individual simulations from Equations (23)-(25). Although the difference between the upper and lower bounds is relatively large (about a factor 5), the simulated results seem qualitatively well-captured by them. Moreover, as these upper and lower bounds are based on individual subset simulations, the upper bound can serve as a conservative first estimate of the accuracy of results obtained by subset simulation. Using the lower bound solution (by assuming no correlation between Markov chains, as proposed by Au and Beck (2001) and used in some publications) seems to underestimate the uncertainty in the calculated probability of failure, as can be concluded from the lower prediction of $CoV_n$ in Figure 7.

The algorithmic efficiency determined over the 100 simulations and expressed in the normalized coefficient of variation $CoV_n$ in Figure 7 can be compared with results in other publications. For reference to the original subset simulation, Li et al. (2016b)obtained $CoV_n = 18.2$ at a probability level of $p_f = 1.7 \times 10^{-4}$ for original subset selection based on the SSR. Meanwhile, Huang et al. (2016) obtained $CoV_n = 34.0$ at a probability level of $p_f \approx 1 \times 10^{-4}$ using direct stability analysis and yield-based subset selection. The results presented in Figure 7 give $CoV_n = 30$ at $p_f = 1 \times 10^{-4}$, suggesting that the proposed method has an algorithmic efficiency comparable with the method proposed by Huang et al. (2016) at probability levels around $1 \times 10^{-4}$.

Figure 9 shows the total number of realizations $N_t$ per subset required to obtain $N_c$ failed realizations (red crosses). This number is directly dependent on the predicted threshold and its ability to capture the target conditional probability $p_0$ over the defined subset. Except for a few outliers, the range of obtained realization numbers $N_t$ (1000 to 4000) corresponds to conditional probabilities in the range 0.05 to 0.20. The choice of the initial strength reduction factors, $f_s^{(1)}$ and $f_s^{(2)}$, proves to be conservative with respect to the target number of realizations per subset.

Although in general two function calls are required for a realization, the effective number of runs is much lower. This is firstly because the existing seeds only need to be analyzed once and secondly because rejected proposal samples of the MCMC do not need to be analyzed a second time. A low acceptance rate of the MMA in MCMC therefore leads to a lower number of function calls per subset.

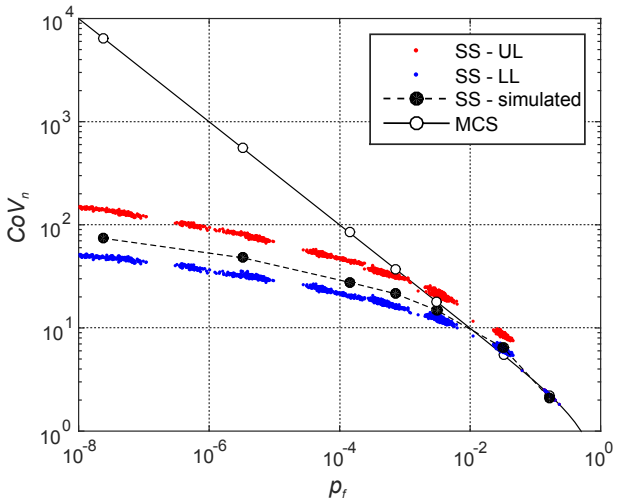


Figure 7: Normalized coefficient of variation $CoV_n$ obtained from 100 runs of SS. Lower and upper limits are determined per simulation at each subset level by (26) and (27) respectively.

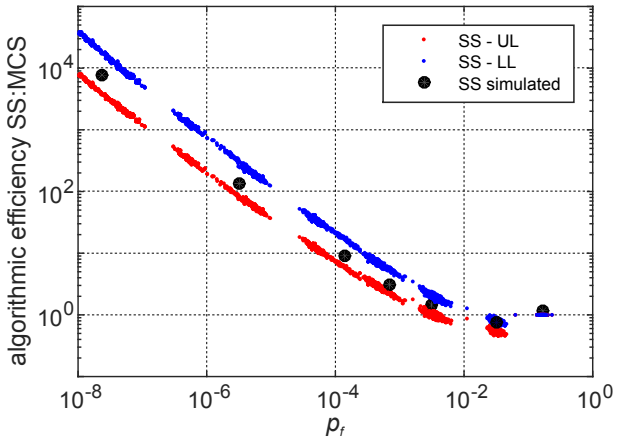


Figure 8: Efficiency of SS relative to MCS at different levels of probability.

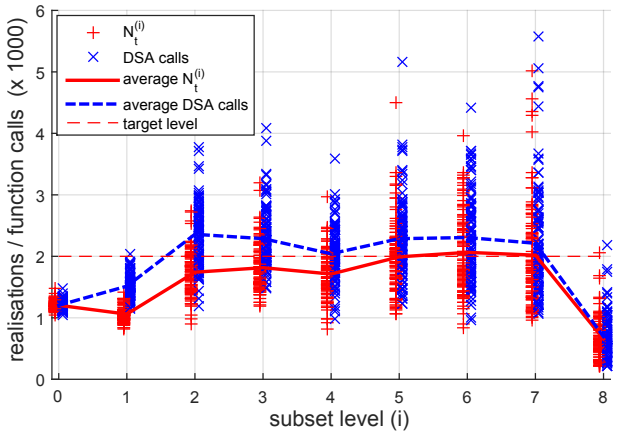


Figure 9: Number of realizations per subset (+) and number of DSA function calls per subset (×) for each simulation. The solid lines indicate the average over 100 simulations.

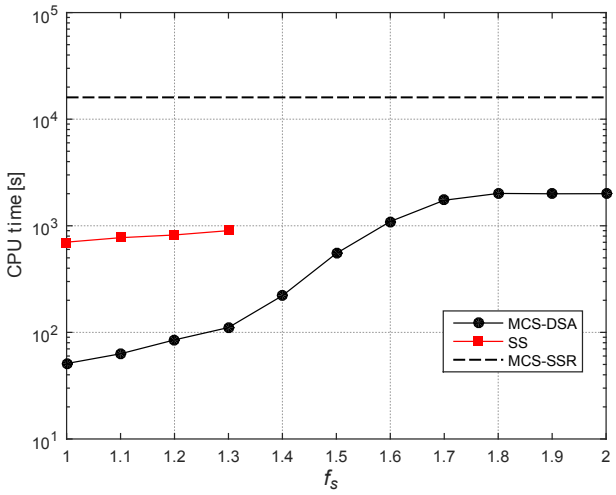


Figure 10: Comparison of computation time required for analyzing 1000 realizations in DSA and SS.

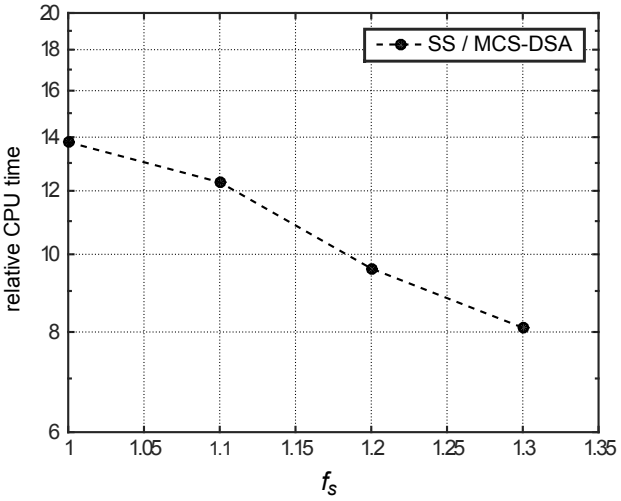


Figure 11: Computation time per FEM call in SS for $FOS < f_s$ relative to MCS-DSA at the corresponding $f_s$.

### *6.2. CPU time efficiency*

The algorithmic efficiency presented in Figure 8 is expressed in the relative number of calls of FEM-DSA and cannot directly be translated into a gain in computation time, as the computation time for a single DSA depends strongly on the amount of plastic yielding to be accounted for in the computation. For stable slopes (with little yielding) the convergence of the numerical solution is efficient; for failing slopes, the modified Newton-Raphson algorithm that is employed does not converge to a solution and the maximum prescribed number of plastic iterations is required for the analysis. The number of times a DSA is performed up to the maximum number of iterations is significantly higher for SS than for direct MCS as more slope failures are evaluated in SS. Figure 10 shows the average computation time required for 1000 FEM calls in MCS-SSR, MCS-DSA and SS for different levels of $f_s$. The computation time for MCS-SSR includes the iterations to find the $FOS$, here at an accuracy of $1 \times 10^{-3}$. The computation times for SS represent simulations up to the given $f_s$, thereby including the required DSA at higher $f_s$ for the intermediate subsets. The relative difference between the computation time in subset simulation and MCS-DSA is given in Figure 11. This relative difference can be used as a correction factor on the algorithmic efficiency to obtain the computation time efficiency of the methods. Table 3 gives the computation time efficiency of SS relative to MCS, corrected for relative computation time with respect to algorithmic efficiencies presented in Table 2. The resulting

| $f_s$ | $p_f$ | alg. eff. | comp. time eff. |
|---|---|---|---|
| 1.30 | $3.11 \times 10^{-3}$ | 1.5 | 0.180 |
| 1.20 | $1.39 \times 10^{-4}$ | 11 | 0.922 |
| 1.10 | $3.22 \times 10^{-6}$ | 140 | 10.09 |
| 1.00 | $2.40 \times 10^{-8}$ | 7823 | 557 |

Table 3: Computation time comparison between SS-DSA and MCS-DSA.

computation time efficiency of the SS thereby becomes negative with respect to MCS for the larger probabilities of failure and equal efficiency is obtained at around $p_f = 1 \times 10^{-4}$. The relative computation time efficiency of SS further increases with decreasing $p_f$ to a few orders of magnitude towards $p_f = 1 \times 10^{-8}$.

Note that the above efficiency analyses are based on a single choice (as an initial guess) of the first two intermediate factors of safety $f_s^{(1)}$ and $f_s^{(2)}$. This choice was not adapted afterwards, although a possible gain in efficiency can be made by optimizing it. The efficiency of subset simulation is further determined by the efficient sampling of uncorrelated realizations in the Markov chains, which also could be optimized (Papadopoulos et al., 2012; Vrugt, 2016).

## 7. Qualitative evaluation of simulated results

Taking account of spatial variability in soil strength parameters is known to introduce a range of possible sliding volumes and sliding depths. Using shear strength reduction, the variation in depth was demonstrated by Hicks et al. (2008) using RFEM simulations. Variation in sliding depth at a strength reduction factor of $f_s = 1.0$ was demonstrated by Wang et al. (2011), using a limit equilibrium method in combination with subset simulations to address the low-probability events. In the following, the results of the subset simulations discussed above are used to evaluate the sliding volumes and sliding depths at different levels of shear strength reduction $f_s$ in order to compare the resulting distributions with those obtained by shear strength reduction.

To determine the sliding mass from the realizations leading to failure at a given strength reduction factor, different methods are available, for example based on ridge-finding techniques applied to deviatoric strain contours or based on the calibrated thresholding of horizontal displacement fields (Hicks et al., 2008). Details on the calibration of the threshold, which is expressed as a percentage of the maximum displacement, are given in Hicks et al. (2014). The $K$-means clustering method (KMCM) (Huang et al., 2013) is employed here. This method divides the nodes into $K_{cl}$ clusters, based on the difference in displacement with respect to the average of the cluster they are part of. In this way, KMCM overcomes the need to calibrate a relative displacement threshold in obtaining an objective definition of sliding volumes.

In the case when $K_{cl} = 2$ clusters are defined, one of the clusters is formed by the nodes in the sliding body, whereas the other is the cluster of nodes outside the sliding body. The division of the nodes into clusters is based on the minimization of an objective term $R$:

$$R = \sum_{k=1}^{K_{cl}} \sum_{\vec{u} \in \Omega^k} \left( |u_i| - |c_i^k| \right) \left( |u_i| - |c_i^k| \right) \tag{30}$$

where $u_i$ is the component $i$ of the nodal displacement vector $\vec{u}$ and $c_i^k$ is the component of the mean displacement vector $\vec{c}^{\,k}$ of cluster $\Omega^k$. The mean displacement vector $\vec{c}^{\,k}$ is defined as the mean of the absolute components of $\vec{u} \in \Omega^k$. The absolute of the individual components is used here to make sure that sliding bodies with rotation as the dominant mode of displacement are not divided into two different clusters. This proves to be a crucial requirement in the analysis of slopes with deep slip surfaces.

The minimization scheme is an iterative process of assigning nodes to either one of the two clusters and updating the cluster average displacement vectors $\vec{c}^{\,k}$ until no further reduction of $R$ can be obtained. An example of the sliding mass determined with the KMCM is shown in Figure 12. It should however be noted that, like other methods, KMCM is not flawless. Some of these flaws show up in Figure 13 as KMCM artifacts, as a result of parts of the sliding body that cannot be identified on total displacement alone. These are generally related to rotational movement of the

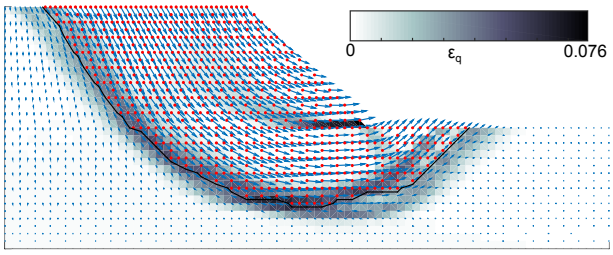


Figure 12: Example of the $K$-means clustering method to identify the sliding mass and the slip surface. Deviatoric strain (grayscale), nodal displacement vectors (blue arrows, not to scale), nodes of sliding body (red dots), determined slip surface (black line).

sliding body with a centre of rotation close to the crest of the slope. Others are influenced by the reflection of shear bands at the left domain boundary or jumps between dominant sliding surfaces. A larger simulation domain, avoiding interaction of the sliding surface with the farfield boundary, generally prevents these latter artifacts from appearing.

Subset simulation provides the means to efficiently generate realizations at low probabilities of failure, such that failing realizations at a predetermined strength reduction can be obtained. This is used to study the conditional modes of failure of the slopes with respect to the factor of safety. Figure 13 shows the slip surfaces obtained from 100 final realizations of both MCS with SSR and subset simulations for different levels of strength reduction factors $FOS < f_s$. The slip surfaces at different conditional levels of $FOS$ demonstrate that the mode of failure strongly varies with the slope $FOS$. Slopes with a low $FOS$ tend to have a shallow failure mechanism, which is different from the predominantly deep failure surfaces that are found as solutions for homogeneous slopes or the solutions from shear strength reduction in MCS.

This effect can be explained by considering the balance of driving and resisting forces. The behaviour of a homogeneous cohesive soil predicts a deep failure surface for the given example, as a result of a less favorable ratio (with respect to stability) between driving forces (gravitational forces on sliding mass) and resistance forces (shear strength along slip surface) in the case of a deep mode of failure. For a slip surface to be feasible in the case of heterogeneity of shear strength, the (average) shear strength along the surface needs to be sufficiently low. Long slip surfaces with a low average shear strength are less likely to naturally occur in random field realizations than short slip surfaces with low average resistance.

The difference in failure modes can further be characterized by evaluating the distribution of the sliding volume (per unit slope length) and depth of the slip surface beneath the toe of the slope for the different cases. The sliding volume per unit length is defined by the area above the failure surface, and is evaluated for all 20,000 realizations for which $FOS \leq f_s^{end}$ as the result of $4 \times 100$ analyses for which $f_s^{end}$ is 1.0, 1.1, 1.2 and 1.3 respectively. Figures 14 and 15 show distributions of sliding volume and slip surface depth for slope failure events at the different conditional levels of strength reduction. Comparison of the sliding volume and slip surface depth for $FOS < 1.0$ with those obtained by SSR shows a fundamental difference in slope response. Clearly, failure events taking place without strength reduction have a different mode of failure than stable slopes that are brought to failure by means of strength reduction and the expected sliding volume appears to be correlated to the $FOS$ of the slope. To better highlight this, the expected sliding volume as a function of the $FOS$ is estimated from the 20,000 realizations of the SSR-MCS. Average sliding volumes are determined for 100 bins in the range $1.0 < FOS < 2.0$ to determine the $FOS$-dependent sliding volume (Figure 16). Note that, in the comparison in this figure, results obtained by SSR represent $FOS \approx f_s$ and results for DSA represent $FOS \leq f_s$. The average over the 20,000 realizations from subset simulations for $FOS \leq f_s = 1.0$, 1.1, 1.2 and 1.3 are also given. Comparison shows that subset simulation continues the trend suggested by the tail of the distribution based on the MCS-SSR. The difference between the expected sliding mass for slopes failing under their own weight (34 $m^3/m$) and the expected sliding volume found by MCS-SSR (87 $m^3/m$) corroborate the fundamental difference between the results of DSA and SSR.

This relation between $FOS$ and sliding volume was earlier suggested based on results from the 3D failure analysis of slopes without a foundation (Hicks et al., 2008; Hicks and Spencer, 2010; Li et al., 2015) and slopes with a foundation layer (Hicks et al., 2014). Although the analyses in these publications are based on 3D sliding volumes with a limited number of realizations, covering only a small range of factors of safety, the suggested trend is consistent with the relation demonstrated in Figure 15; heterogeneous slopes with a smaller factor of safety $FOS$ have a smaller

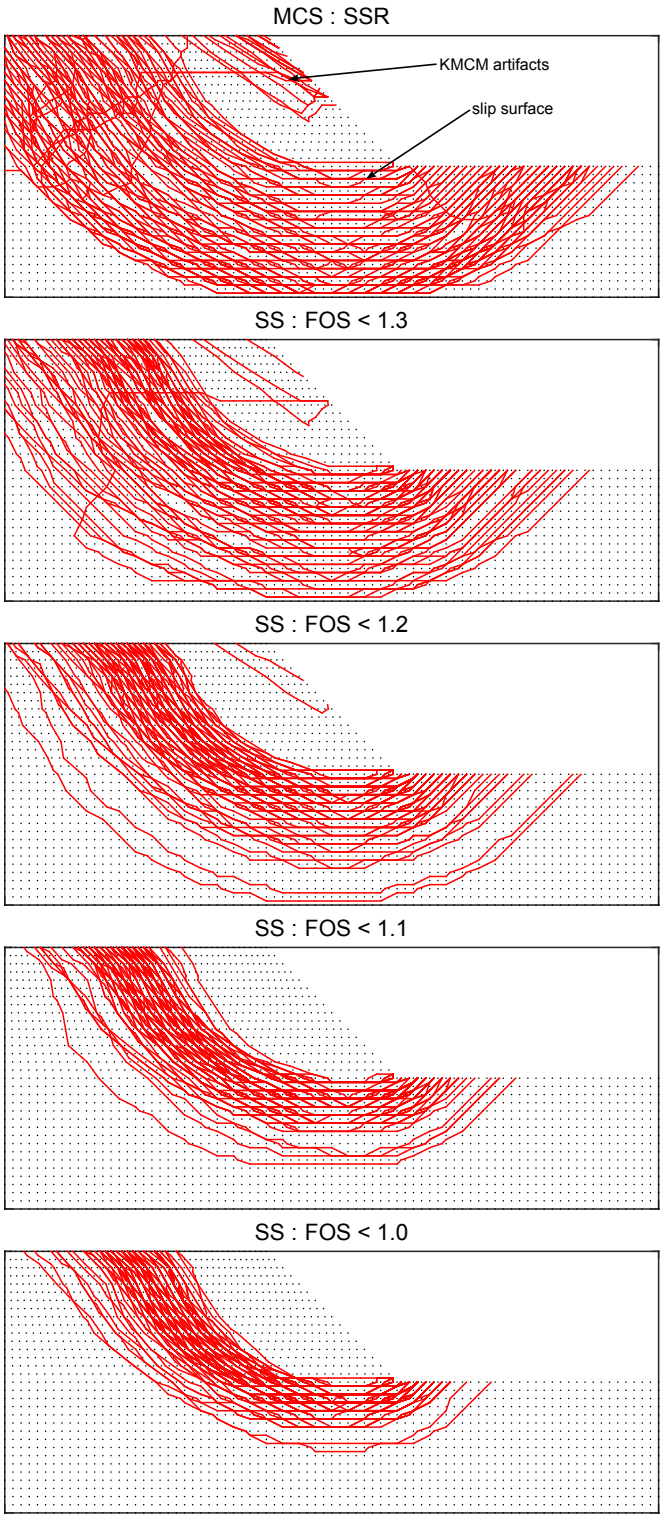


Figure 13: Failure surfaces for 100 realizations generated with subset simulation for different strength reduction factors. The failure surface is the boundary of the sliding body determined using the $K$-means clustering method.

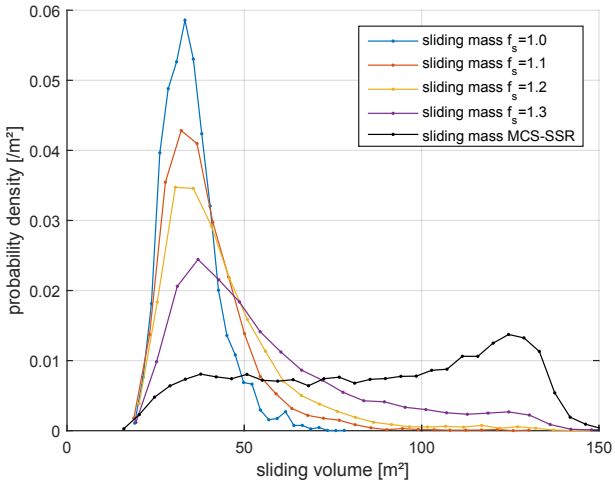


Figure 14: Probability density of sliding volume for different strength reduction factors obtained by SS. Each distribution is based on 20,000 realizations from the 100 subset simulations.

expected siding volume.

It can be expected that the analysis of low probability failure events in 3D simulations, taking account of spatial variability of strength parameters, shows a stronger discrepancy in sliding volumes between the results of SS-DSA and MCS-SSR. This effect can have a major impact in the risk assessment of slopes, in which the consequence of failure is strongly related to the sliding volume.

The relation between the mode of failure and the factor of safety has another important consequence; the use of parameters related to the mode of failure for the selection of subset seeds, might lead to biased results with respect to modes of failure. Hence, a method of subset selection consistent with the original subset simulation is required to obtain comparable unbiased and ergodic properties. This consistency is here maintained by the performance-based subset selection, with failure/no-failure performance as an order-preserving indicator of $FOS$. Although the obtained conditional level of probability $\mathrm{P}(F^{(i)}|F^{(i-1)})$ does differ from the target $p_0$, the ergodic and bias properties are considered similar to the original subset simulation, with asymptotic ergodicity and unbiasedness for an increasing subset sample size $N_c$. For further discussion on the sensitivity of parameter choice in subset simulation in general, the reader is referred to Au and Wang (2014).

## 8. Conclusion

A modified version of subset simulation in combination with MCMC simulation for slope stability analysis is proposed. This version overcomes the need for computationally expensive evaluation of the exact factor of safety. The subset simulation algorithm is changed from the usual probability-based subset selection to a criterion-based subset selection. From a prediction of the failure probability curve, subsequent threshold strength reduction factors can be selected without the need of ranking the realizations. This leads to a computationally efficient algorithm with a fully consistent subset selection criterion.

Simulations demonstrate the efficiency of the new scheme to be high in comparison with direct stability analysis in crude Monte-Carlo methods when addressing failure events with small probabilities. Algorithmic efficiency of the proposed subset simulation approach was demonstrated to be higher than Monte Carlo simulation using direct stability analysis for addressing probabilities of failure $p_f < 0.01$. When it comes to CPU-time efficiency, subset simulation was found to be more efficient than Monte Carlo simulations for $p_f < 1 \times 10^{-4}$.

Presented results have demonstrated the need for a careful and consistent evaluation of slope failure mechanisms. In fact, the evaluation of failure mechanisms that are triggered in initially stable slopes by strength reduction techniques was demonstrated to lead to an overestimation of the sliding volume. Although shear strength reduction might be applicable in stability analyses of homogeneous slopes, the demonstrated differences in failure mechanism in the case of spatially variable soils suggests that strength reduction may not be applicable as a general approach to

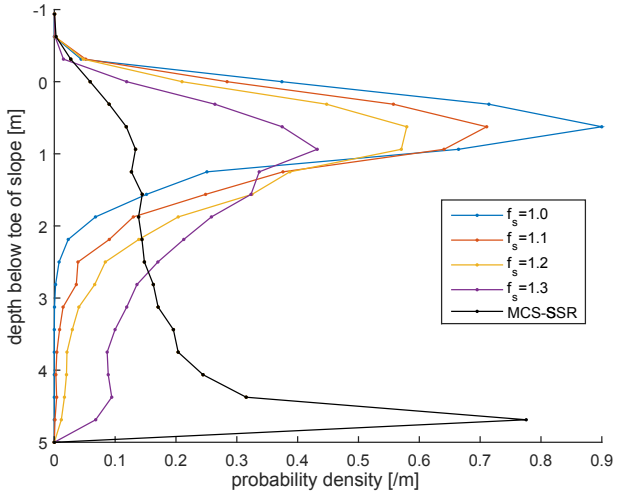


b)

Figure 15: Probability density of slip surface depth for different levels $FOS < f_s$ over the 20,000 realizations obtained by SS.

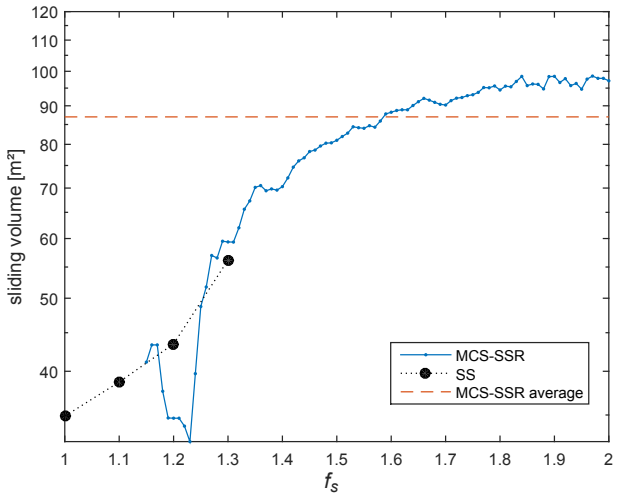


Figure 16: Expectation of sliding volume as a function of critical strength reduction factor $f_s$.

evaluating the modes of failure in heterogeneous soils. This not only has consequences for the application of shear strength reduction in risk assessments, but also questions the application of partial factors to correct for uncertainties in parameters that show spatial variability.

## Acknowledgements

This research is supported under project number 13864 by the Dutch Technology Foundation STW, which is part of the Netherlands Organisation for Scientific Research (NWO).

## Bibliography

Ahmed, A., Soubra, A.-H., 2012. Probabilistic analysis of strip footings resting on a spatially random soil using subset simulation approach. Georisk: Assessment and Management of Risk for Engineered Systems and Geohazards 6 (3), 188–201.

Arnold, P., Hicks, M. A., 2011. A stochastic approach to rainfall-induced slope failure. In: Proceedings of 3rd Int Symp Safety and Risk, Munich, Germany. pp. 107–115.

Au, S.-K., Beck, J. L., 2001. Estimation of small failure probabilities in high dimensions by subset simulation. Probabilistic Engineering Mechanics 16 (4), 263–277.

Au, S.-K., Wang, Y., 2014. Engineering risk assessment with subset simulation. John Wiley & Sons.

Baecher, G. B., Christian, J. T., 2005. Reliability and statistics in geotechnical engineering. John Wiley & Sons.

Christian, J. T., Baecher, G. B., 1999. Point-estimate method as numerical quadrature. Journal of Geotechnical and Geoenvironmental Engineering 125 (9), 779–786.

Deutsch, C. V., Journel, A. G., 1998. GSLIB: Geostatistical Software Library and User's Guide, 2nd Edition. Oxford Univ. Press, New York.

Fenton, G. A., 1994. Error evaluation of three random-field generators. Journal of Engineering Mechanics 120 (12), 2478–2497.

Fenton, G. A., Griffiths, D. V., 2002. Probabilistic foundation settlement on spatially random soil. Journal of Geotechnical and Geoenvironmental Engineering 128 (5), 381–390.

Fenton, G. A., Vanmarcke, E. H., 1990. Simulation of random fields via local average subdivision. Journal of Engineering Mechanics 116 (8), 1733–1749.

Green, D. K. E., Douglas, K., Mostyn, G., 2015. The simulation and discretisation of random fields for probabilistic finite element analysis of soils using meshes of arbitrary triangular elements. Computers and Geotechnics 68, 91–108.

Griffiths, D. V., Fenton, G. A., 2004. Probabilistic slope stability analysis by finite elements. Journal of Geotechnical and Geoenvironmental Engineering 130 (5), 507–518.

Griffiths, D. V., Huang, J., Fenton, G. A., 2009. Influence of spatial variability on slope reliability using 2-d random fields. Journal of Geotechnical and Geoenvironmental Engineering 135 (10), 1367–1378.

Hicks, M. A., Chen, J., Spencer, W. A., May 2008. Influence of spatial variability on 3d slope failures. In: Brebbia, C. A., Beriatos, E. (Eds.), Proceedings of the 6th International Conference on Computer Simulation in Risk Analysis and Hazard Mitigation. Cephalonia, Greece. pp. 335–342.

Hicks, M. A., Nuttall, J. D., Chen, J., 2014. Influence of heterogeneity on 3d slope reliability and failure consequence. Computers and Geotechnics 61, 198–208.

Hicks, M. A., Samy, K., 2002. Influence of heterogeneity on undrained clay slope stability. Quarterly Journal of Engineering Geology and Hydrogeology 35 (1), 41–49.

Hicks, M. A., Spencer, W. A., 2010. Influence of heterogeneity on the reliability and failure of a long 3d slope. Computers and Geotechnics 37 (7), 948–955.

Huang, J., Fenton, G. A., Griffiths, D. V., Li, D. Q., Zhou, C.-B., 2016. On the efficient estimation of small failure probability in slopes. Landslides, doi:10.1007/s10346–016–0726–2.

Huang, J., Lyamin, A. V., Griffiths, D. V., Krabbenhoft, K., Sloan, S. W., 2013. Quantitative risk assessment of landslide by limit analysis and random fields. Computers and Geotechnics 53, 60–67.

Huang, S. P., Quek, S. T., Phoon, K.-K., 2001. Convergence study of the truncated Karhunen-Loeve expansion for simulation of stochastic processes. International journal for numerical methods in engineering 52 (9), 1029–1043.

Jiang, S.-H., Huang, J., Zhou, C.-B., 2017. Efficient system reliability analysis of rock slopes based on subset simulation. Computers and Geotechnics 82, 31–42.

Jiang, S.-H., Huang, J.-S., 2016. Efficient slope reliability analysis at low-probability levels in spatially variable soils. Computers and Geotechnics 75, 18–27.

Li, C.-C., Der Kiureghian, A., 1993. Optimal discretization of random fields. Journal of Engineering Mechanics 119 (6), 1136–1154.

Li, D.-Q., Xiao, T., Cao, Z.-J., Phoon, K.-K., Zhou, C.-B., 2016a. Efficient and consistent reliability analysis of soil slope stability using both limit equilibrium analysis and finite element analysis. Applied Mathematical Modelling 40 (9), 5216–5229.

Li, D.-Q., Xiao, T., Cao, Z.-J., Zhou, C.-B., Zhang, L.-M., 2016b. Enhancement of random finite element method in reliability analysis and risk assessment of soil slopes using subset simulation. Landslides 13 (2), 293–303.

Li, Y. J., Hicks, M. A., Nuttall, J. D., 2015. Comparative analyses of slope reliability in 3d. Engineering Geology 196, 12–23.

Metropolis, N., Rosenbluth, A. W., Rosenbluth, M. N., Teller, A. H., Teller, E., 1953. Equation of state calculations by fast computing machines. Journal of Chemical Physics 21 (6), 1087–1092.

Papadopoulos, V., Giovanis, D. G., Lagaros, N. D., Papadrakakis, M., 2012. Accelerated subset simulation with neural networks for reliability analysis. Computer Methods in Applied Mechanics and Engineering 223, 70–80.

Papaioannou, I., Betz, W., Zwirglmaier, K., Straub, D., 2015. MCMC algorithms for subset simulation. Probabilistic Engineering Mechanics 41, 89–103.

Rosenblueth, E., 1975. Point estimates for probability moments. Proceedings of the National Academy of Sciences 72 (10), 3812–3814.

Smith, I. M., Griffiths, D. V., Margetts, L., 2013. Programming the finite element method. John Wiley & Sons.

Suchomel, R., Mašín, D., 2011. Probabilistic analyses of a strip footing on horizontally stratified sandy deposit using advanced constitutive model. Computers and Geotechnics 38 (3), 363–374.

Sudret, B., Der Kiureghian, A., 2000. Stochastic finite element methods and reliability: a state-of-the-art report. Department of Civil and Environmental Engineering, University of California Berkeley, CA.

Vanmarcke, E., 1983. Random fields: Analysis and synthesis. MIT Press, Cambridge, MA.

Vrugt, J. A., 2016. Markov chain Monte Carlo simulation using the DREAM software package: Theory, concepts, and matlab implementation. Environmental Modelling & Software 75, 273–316.

Wang, Y., Cao, Z.-J., Au, S.-K., 2011. Practical reliability analysis of slope stability by advanced Monte Carlo simulations in a spreadsheet. Canadian Geotechnical Journal 48 (1), 162–172.

Xiao, T., Li, D.-Q., Cao, Z.-J., Au, S.-K., Phoon, K.-K., 2016. Three-dimensional slope reliability and risk assessment using auxiliary random finite element method. Computers and Geotechnics 79, 146–158.